Lithuanian Journal of Physics
Vol. **66**, No. 2, pp. 107–112 (2026)
ISSN 1648-8504 eISSN 2424-3647
DOI: https://doi.org/10.3952/physics.2026.66.2.5

EPR OF X-RAY-IRRADIATED $[(CH_3)_2NH_2][Zn(HCOO)_3]$ HYBRID PEROVSKITE

G. Usevičius [a], I. Pocius [a], R. Dobužinskas [b], M. Mączka [c], G. Sliaužys [b], J. Banys [a], and M. Šimėnas [a]

[a] *Institute of Applied Electrodynamics and Telecommunications, Faculty of Physics, Vilnius University, Saulėtekio 3, 10257 Vilnius, Lithuania*

[b] *Institute of Chemical Physics, Faculty of Physics, Vilnius University, Saulėtekio 3, 10257 Vilnius, Lithuania*

[c] *Institute of Low Temperature and Structure Research, Polish Academy of Sciences, PL-50-422 Wroclaw, Poland*

Email: gediminas.usevicius@ff.vu.lt

Received 7 January 2026; accepted 21 January 2026

Incorporating paramagnetic metal ions into hybrid materials is a standard practice to enable electron paramagnetic resonance (EPR) studies of phase transitions and dynamics. Yet, the inclusion of foreign ions in the lattice can significantly distort the local structure, resulting in the inaccurate understanding of the material properties. Less invasive paramagnetic defects can be formed by high energy irradiation. Here, we report a continuous-wave (CW) EPR study of X-ray-irradiated $[(CH_3)_2NH_2][Zn(HCOO)_3]$ hybrid perovskite, which possesses a structural phase transition at ~160 K. The CW EPR spectrum reveals a rhombic $\boldsymbol{g}$-tensor with no clearly resolved hyperfine splittings. Assisted by the DFT calculations, we assign the spectrum to a radical species on the formate linker. The temperature dependence of the measured g_{zz} component reveals a broad anomaly in a broad temperature range close to the phase transition point, which we relate to the change in the dynamics of a formate linker.

Keywords: EPR, hybrid perovskite, phase transition

1. Introduction

Lately, hybrid organic–inorganic materials have gained a significant scientific attention [1–3]. The interest in hybrid compounds is due to their versatile chemical and physical properties originating from a vast variety of possible organic and inorganic moieties. The main possible applications of these hybrid materials include efficient solar cells [4, 5], multiferroic memories [6, 7], gas storage devices [8], and catalysis [9].

One of the most researched hybrid material group is formate perovskites [2, 10–17], $[A][M(HCOO)_3]$, where A denotes an alkyl-ammonium cation and M is a divalent metal ion. These hybrid materials typically possess structural phase transitions, which are usually connected with the emergence of ferroelectric and dynamic phenomena [10, 13, 16–22].

Among various experimental techniques, electron paramagnetic resonance (EPR) spectroscopy has emerged as a particularly powerful tool for probing local structural changes associated with phase transitions and dynamics in hybrid materials [13–17, 20, 23–27]. However, the majority of hybrid materials do not have intrinsic paramagnetic centres. Thus, typically, a small amount of paramagnetic transition metal ions is incorporated into a structure acting as local spin probes. Despite the success of EPR for investigating hybrid materials, the incorporation of guest ions may distort the local structure, complicating the interpretation of phase transitions and dynamical processes. Such effects are especially pronounced for Jahn–Teller-active ions such as Cu^{2+} [13, 20, 28].

Paramagnetic defects created by high-energy irradiation are typically less invasive and provide access to less perturbed dynamic and structural

information [29–31]. Here, we use X-ray irradiation to create spin probes in the inorganic framework of $[(CH_3)_2NH_2][Zn(HCOO)_3]$ (DMAZn) hybrid perovskite, which exhibits a structural phase transition at ~160 K [18, 32]. We perform X-band continuous-wave (CW) EPR spectroscopy to explore the created radical and its response to the structural phase transition of DMAZn.

2. Experimental and simulation details

2.1. Sample preparation

$ZnCl_2$ (99.999%, *Sigma-Aldrich*), a 2.0 M solution of dimethylamine in methanol (*Sigma-Aldrich*), methanol (99.8%, *Sigma-Aldrich*) and formic acid (98%, *Fluka*, Switzerland) were commercially available and used without further purification. Crystals of DMAZn were grown by a slow diffusion method. Namely, 2.5 mL of the 2.0 M solution of dimethylamine in methanol and 0.5 mL of formic acid were added to 10 mL of methanol. This solution was placed at the bottom of a glass tube (20 mm inner diameter). To this solution, 2 mL of methanol was layered, followed by 20 mL of the methanol solution containing 1 mmol of $ZnCl_2$. The tube was sealed and kept undisturbed. The colourless crystals were harvested after 3 days, washed three times with methanol, and dried at room temperature.

2.2. X-ray exposure

X-ray irradiation was conducted at room temperature using a BSV-2 vacuum X-ray tube integrated with the high-voltage generator of a *Rigaku* SmartLab system. The tube was operated at a constant accelerating potential of 60 kV and 30 mA, corresponding to 1.8 kW electrical power deposited into the anode. Tube voltage and current were continuously monitored by the SmartLab control electronics and remained stable throughout the exposure. The BSV-2 tube employed a copper anode, generating a polychromatic bremsstrahlung spectrum with characteristic Cu K_α (≈8.04 keV) and K_β (≈8.90 keV) emission lines. The emitted radiation passed through the tube's beryllium window (inherent filtration) and an unobstructed 25 cm air path before reaching the sample, without an additional filtration, slits, or collimation; X-ray divergence from the focal spot defined the illumination field.

The synthesized DMAZn crystals were grounded into a fine powder and placed into a 4 mm outer diameter EPR tube. The dose rate at the sample position was determined via alanine dosimetry and subsequent EPR spectral readout, yielding an air-kerma-equivalent dose rate that resulted in a total accumulated dose of ≈12,000 Gy for the full 19 h 16 min irradiation.

2.3. EPR spectroscopy

The irradiated sample was placed into an unirradiated 4 mm outer-diameter EPR tube for measurements at X-band (9.5 GHz) frequency. We used a *Bruker* ELEXSYS E580 spectrometer equipped with a high-Q ER4122SHQE microwave resonator. A helium flow cryostat was used to stabilize the temperature. For experiments, we used the 1 G and 100 kHz amplitude and frequency of the modulation field, respectively. The microwave power was adjusted to avoid the saturation of the EPR signal.

2.4. Simulation details

We used EasySpin 6.0.10 [33] running on MATLAB R2021b (*The MathWorks Inc.*) to simulate the CW EPR spectra.

Density functional theory calculations of EPR parameters were performed using the ORCA 5.0.4 package. The B3LYP hybrid functional and the EPR-II basis set were employed. The resolution-of-identity approximation with the automatically generated auxiliary basis sets (AutoAux) was used to improve computational efficiency.

3. Results and discussion

First, we measured the room-temperature X-band CW EPR spectrum (Fig. 1(a)) of the irradiated DMAZn sample to confirm the creation of the radical species. The observed EPR signal is typical for a spin Hamiltonian with a rhombic $\boldsymbol{g}$-tensor with no clearly resolved hyperfine splittings. We simulated the experimental spectrum and determined the principal components of the $\boldsymbol{g}$-tensor: g_{xx} = 1.99695(5), g_{yy} = 2.0023(4) and g_{zz} = 2.0028(2). The resulting simulated spectrum is in a good agreement with the experiment (Fig. 1(a)).

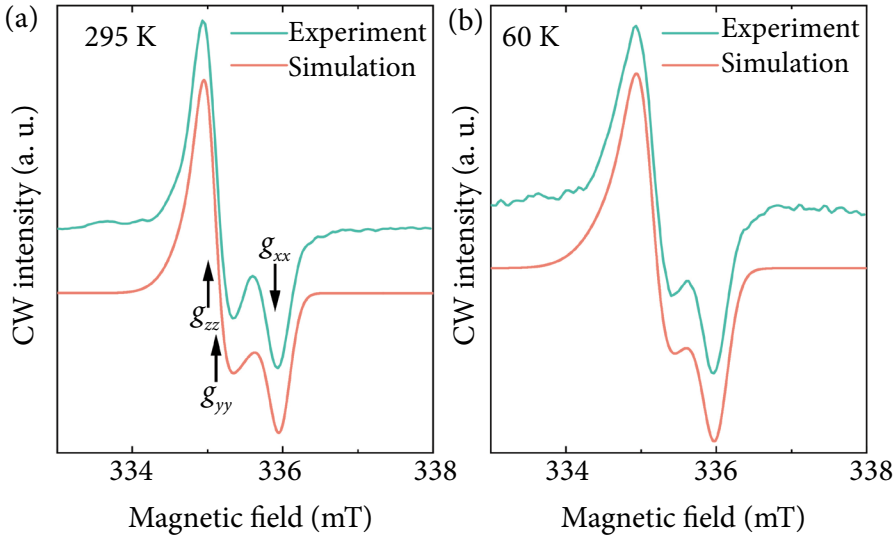

Fig. 1. The measured (turquoise) and simulated (red) CW EPR spectrum of radical spins in X-ray-irradiated DMAZn obtained at (a) 295 and (b) 60 K.

To determine the origin of the EPR signal, we performed density functional theory (DFT) calculations on three possible radical species in this compound: carbon- or nitrogen-centred radical on the DMA cation and carbon-centred radical on the formate linker. Contrary to the experimental observations, our DFT calculations for radical species on the DMA cation revealed substantial ^{1}H and ^{14}N hyperfine splittings. However, the calculations for a formate radical show the absence of the hyperfine splittings, and the calculated $\boldsymbol{g}$-tensor is $g_{\mathrm{DFT},xx}$ = 1.99823, $g_{\mathrm{DFT},yy}$ = 2.0018 and $g_{\mathrm{DFT},zz}$ = 2.0035, which is in a relatively good agreement with the experiment. Thus, our calculations confirm that the observed spectrum corresponds to a radical species formed on the carbon atom of the formate linker by the removal of the proton from the C–H roup.

Temperature-dependent CW EPR spectra were recorded to study how the structural phase transition at T_0 ~ 160 K in DMAZn [17–22] affects the radical signal (Fig. 2). As seen in Fig. 1(b), there are only small differences in the signal between 295 and 60 K spectra suggesting that the spectrum is weakly affected by the ordering of the system, and such a trend is observed throughout the whole measured temperature range. Thus, in contrast to metal centres such as Mn^{2+} and Cu^{2+} [20, 21], the radical species is only weakly sensitive to structural phase transition in DMAZn.

In order to get a full picture of the temperature dependence of a radical signal, the principal components of $\boldsymbol{g}$-tensor are plotted with respect to temperature in Fig. 3. g_{xx} and g_{yy} components remain mainly constant between 60 and 295 K, while the g_{zz} value has a broad anomaly in the temperature range between 146 and 180 K. Due to the radical being positioned at the formate linker, we associate this anomaly with the slowing-down of formate linker dynamics around the phase transition point.

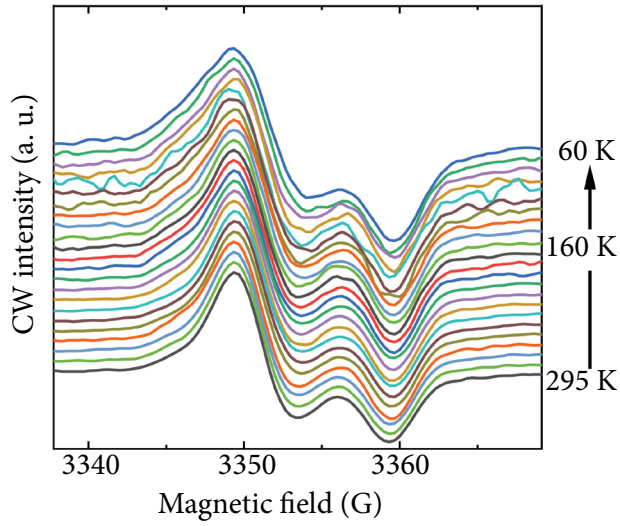

Fig. 2. The temperature dependence of the CW EPR spectrum of radical spins in X-ray-irradiated DMAZn.

4. Summary and conclusions

In this work, we used X-ray irradiation to generate paramagnetic centres in DMAZn hybrid perovskite. Our DFT calculations and CW EPR

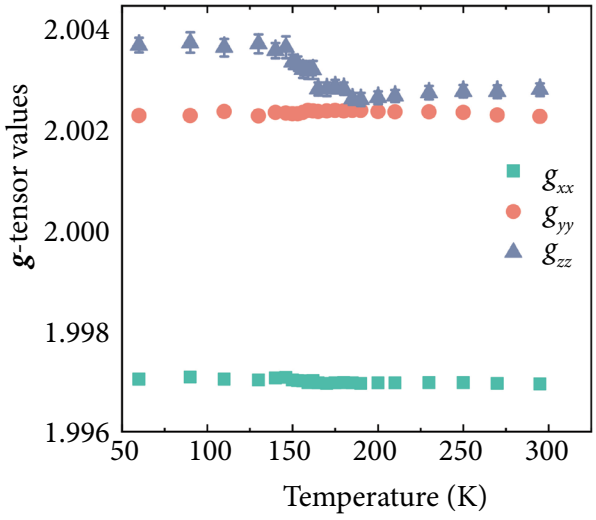

Fig. 3. The temperature dependence of the principal components of the ***g***-tensor of radical spins in X-ray-irradiated DMAZn.

experiments revealed that the radical is created on the formate linker. In contrast to metal ion paramagnetic centres, we observed a weak sensitivity of the radical EPR spectrum to the structural phase transition in DMAZn, where only a slight increase in g_{zz} is observed between 180 and 146 K on cooling. This behaviour is likely related to the slowing dynamics of the organic linker of the DMAZn framework.

In general, our results show a successful creation of the EPR-active radical species in DMAZn. The established radical spins in the structure are potential spin probes to study methyl group tunnelling in DMAZn [24, 25] without distorting the structure by doping it with paramagnetic metal ions.

Acknowledgement

This project has been funded by the Research Council of Lithuania (LMTLT) (Agreement No. P-ITP-25-4).

References

[1] M.J. Rosseinsky, Recent developments in metal–organic framework chemistry: Design, discovery, permanent porosity and flexibility, Micropor. Mesopor. Mater. **73**, 15–30 (2004).

[2] M. Ptak, A. Sieradzki, M. Šimėnas, and M. Mączka, Molecular spectroscopy of hybrid organic–inorganic perovskites and related compounds, Coord. Chem. Rev. **448**, 214180 (2021).

[3] B. Saparov and D.B. Mitzi, Organic–inorganic perovskites: Structural versatility for functional materials design, Chem. Rev. **116**(7), 4558–4596 (2016).

[4] J. Jeong, M. Kim, J. Seo, H. Lu, P. Ahlawat, A. Mishra, Y. Yang, M.A. Hope, F.T. Eickemeyer, M. Kim, et al., Pseudo-halide anion engineering for α-$FAPbI_3$ perovskite solar cells, Nature **592**, 381–385 (2021).

[5] J. Park, J. Kim, H.-S. Yun, M.J. Paik, E. Noh, H.J. Mun, M.G. Kim, T.J. Shin, and S.I. Seok, Controlled growth of perovskite layers with volatile alkylammonium chlorides, Nature **616**, 724–730 (2023).

[6] M. Guo, H.-L. Cai, and R.-G. Xiong, Ferroelectric metal organic framework (MOF), Inorg. Chem. Commun. **13**, 1590–1598 (2010).

[7] K. Asadi and M. van der Veen, Ferroelectricity in metal–organic frameworks: Characterization and mechanisms, Eur. J. Inorg. Chem. **2016**, 4332–4344 (2016).

[8] L.J. Murray, M. Dincă, and J.R. Long, Hydrogen storage in metal–organic frameworks, Chem. Soc. Rev. **38**, 1294–1314 (2009).

[9] J. Lee, O.K. Farha, J. Roberts, K.A. Scheidt, S.T. Nguyen, and J.T. Hupp, Metal–organic framework materials as catalysts, Chem. Soc. Rev. **38**, 1450–1459 (2009).

[10] W. Li, Z. Wang, F. Deschler, S. Gao, R.H. Friend, and A.K. Cheetham, Chemically diverse and multifunctional hybrid organic–inorganic perovskites, Nat. Rev. Mater. **2**, 16099 (2017).

[11] M. Mączka, A. Gągor, M. Ptak, W. Paraguassu, T.A. da Silva, A. Sieradzki, and A. Pikul, Three-dimensional perovskite methylhydrazinium lead chloride with two polar phases and unusual second-harmonic generation bistability above room temperature, Chem. Mater. **29**, 2264–2275 (2017).

[12] M. Sánchez-Andújar, S. Presedo, S. Yáñez-Vilar, S. Castro-García, J. Shamir, and M.A. Señarís-Rodríguez, Characterization of the order–disorder dielectric transition in the hybrid organic–inorganic perovskite-like formate

$Mn(HCOO)_3[(CH_3)_2NH_2]$, Inorg. Chem. **49**, 1510–1516 (2010).

[13] M. Šimėnas, A. Ciupa, M. Mączka, G. Völkel, A. Pöppl, and J. Banys, EPR of structural phase transition in manganese- and copper-doped formate framework of $[NH_3(CH_2)_4NH_3][Zn(HCOO)_3]_2$, J. Phys. Chem. C **120**, 19734–19742 (2016).

[14] M. Šimėnas, S. Balčiūnas, M. Trzebiatowska, M. Ptak, M. Mączka, G. Völkel, A. Pöppl, and J. Banys, Electron paramagnetic resonance and electric characterization of a $[CH_3NH_2NH_2][Zn(HCOO)_3]$ perovskite metal formate framework, J. Mater. Chem. C **5**, 4526–4536 (2017).

[15] M. Navickas, L. Girūnas, V. Kalendra, T. Biktagirov, U. Gerstmann, W.G. Schmidt, M. Mączka, A. Pöppl, J. Banys, and M. Šimėnas, Electron paramagnetic resonance study of ferroelectric phase transition and dynamic effects in a Mn^{2+}-doped $[NH_4][Zn(HCOO)_3]$ hybrid formate framework, Phys. Chem. Chem. Phys. **22**, 8513–8521 (2020).

[16] S. Bertaina, N. Abhyankar, M. Orio, and N.S. Dalal, Measuring motional dynamics of $[(CH_3)_2NH_2]^+$ in the perovskite-like metal–organic framework $[(CH_3)_2NH_2][Zn(HCOO)_3]$: The value of low-frequency electron paramagnetic resonance, J. Phys. Chem. C **122**, 16431–16436 (2018).

[17] M. Orio, J.K. Bindra, J. van Tol, M. Giorgi, N.S. Dalal, and S. Bertaina, Quantum dynamics of Mn^{2+} in dimethylammonium magnesium formate $[(CH_3)_2NH_2][Mg(HCOO)_3]$ studied by multifrequency electron spin resonance, J. Chem. Phys. **154**, 154201 (2021).

[18] P. Jain, N.S. Dalal, B.H. Toby, H.W. Kroto, and A.K. Cheetham, Order–disorder antiferroelectric phase transition in a hybrid inorganic–organic framework with the perovskite architecture, J. Am. Chem. Soc. **130**, 10450–10451 (2008).

[19] P. Peksa, A. Nowok, F. Formalik, J.K. Zaręba, J. Trzmiel, A. Gągor, M. Mączka, and A. Sieradzki, More complex than originally thought: Revisiting the origins of the relaxation processes in dimethylammonium zinc formate, J. Mater. Chem. C **10**, 6866–6877 (2022).

[20] M. Šimėnas, A. Ciupa, G. Usevičius, K. Aidas, D. Klose, G. Jeschke, M. Mączka, G. Völkel, A. Pöppl, and J. Banys, Electron paramagnetic resonance of a copper-doped $[(CH_3)_2NH_2][Zn(HCOO)_3]$ hybrid perovskite framework, Phys. Chem. Chem. Phys. **20**, 12097–12105 (2018).

[21] M. Šimėnas, A. Ciupa, M. Mączka, A. Pöppl, and J. Banys, EPR study of structural phase transition in manganese-doped $[(CH_3)_2NH_2][Zn(HCOO)_3]$ metal–organic framework, J. Phys. Chem. C **119**, 24522–24528 (2015).

[22] M. Šimėnas, S. Balčiūnas, A. Ciupa, L. Vilčiauskas, D. Jablonskas, M. Kinka, A. Sieradzki, V. Samulionis, M. Mączka, and J. Banys, Elucidation of dipolar dynamics and the nature of structural phases in the $[(CH_3)_2NH_2][Zn(HCOO)_3]$ hybrid perovskite framework, J. Mater. Chem. C **7**, 6779–6785 (2019).

[23] M. Šimėnas, A. Kultaeva, S. Balčiūnas, M. Trzebiatowska, D. Klose, G. Jeschke, M. Mączka, J. Banys, and A. Pöppl, Single crystal electron paramagnetic resonance of dimethylammonium and ammonium hybrid formate frameworks: Influence of external electric field, J. Phys. Chem. C **121**, 16533–16540 (2017).

[24] M. Šimėnas, D. Klose, M. Ptak, K. Aidas, M. Mączka, J. Banys, A. Pöppl, and G. Jeschke, Magnetic excitation and readout of methyl group tunnel coherence, Sci. Adv. **6**, eaba1517 (2020).

[25] G. Usevičius, A. Eggeling, I. Pocius, V. Kalendra, D. Klose, M. Mączka, A. Pöppl, J. Banys, G. Jeschke, and M. Šimėnas, Probing methyl group tunneling in $[(CH_3)_2NH_2][Zn(HCOO)_3]$ hybrid perovskite using Co^{2+} EPR, Molecules **28**, 979 (2023).

[26] G. Usevičius, J. Turčak, Y. Zhang, A. Eggeling, Ž. Einorytė, M.A. Hope, Š. Svirskas, D. Klose, V. Kalendra, K. Aidas, G. Jeschke, J. Banys, and M. Šimėnas, Probing structural and dynamic properties of $MAPbCl_3$ hybrid perovskite using Mn^{2+} EPR, Dalton Trans. **53**, 7292–7302 (2024).

[27] M. Ptak, A. Kabański, B. Dziuk, S. Balčiūnas, G. Usevičius, J.K. Zaręba, J. Banys, M. Šimėnas, A. Sieradzki, and D. Stefańska, Mechanism of isosymmetric polar order–disorder phase transition

in pyroelectric $[CH_3CH_2NH_3]_2NaGa(HCOO)_6$ double perovskite, J. Mater. Chem. C **12**, 4663–4675 (2024).

[28] P. Peksa, J. Trzmiel, K. Fedoruk, A. Gągor, M. Šimėnas, A. Ciupa, S. Pawlus, J. Banys, M. Mączka, and A. Sieradzki, Impact of the copper-induced local framework deformation on the mechanism of structural phase transition in $[(CH_3)_2NH_2][Zn(HCOO)_3]$ hybrid metal–formate perovskite, J. Phys. Chem. C **123**, 23594–23603 (2019).

[29] R. Krzyminiewski, A. Bielewicz-Mordalska, and R.M. Kowalczyk, Radicals as probes of ferroelectric phase transitions in EPR investigations of pyridinium tetrafluoroborate, J. Magn. Reson. **135**, 76–81 (1998).

[30] J. Gaillard, O. Constantinescu, and B. Lamotte, ESR of free radicals in ferroelectric and antiferroelectric arsenate single crystals, J. Chem. Phys. **55**, 5447–5452 (1971).

[31] B. Lamotte, J. Gaillard, and O. Constantinescu, ESR identification of Slater configurations and of exchange of the $(AsO_4)^{4-}$ radical in irradiated ferroelectric KH_2AsO_4 and KD_2AsO_4 and antiferroelectric $NH_4H_2AsO_4$ and $ND_4D_2AsO_4$, J. Chem. Phys. **57**, 3319–3329 (1972).

[32] T. Asaji and K. Ashitomi, Phase transition and cationic motion in a metal–organic perovskite, dimethylammonium zinc formate $[(CH_3)_2NH_2][Zn(HCOO)_3]$, J. Phys. Chem. C **117**, 10185–10190 (2013).

[33] S. Stoll and A. Schweiger, EasySpin, a comprehensive software package for spectral simulation and analysis in EPR, J. Magn. Reson. **178**, 42–55 (2006).

RENTGENO SPINDULIAIS APŠVITINTO $[(CH_3)_2NH_2][Zn(HCOO)_3]$ HIBRIDINIO PEROVSKITO EPR TYRIMAS

G. Usevičius [a], I. Pocius [a], R. Dobužinskas [b], M. Mączka [c], G. Sliaužys [b], J. Banys [a], M. Šimėnas [a]

[a] *Vilniaus universiteto Fizikos fakulteto Taikomosios elektrodinamikos ir telekomunikacijų institutas, Vilnius, Lietuva*

[b] *Vilniaus universiteto Fizikos fakulteto Cheminės fizikos institutas, Vilnius, Lietuva*

[c] *Lenkijos mokslų akademijos Žemų temperatūrų ir struktūros tyrimų institutas, Vroclavas, Lenkija*

Santrauka

Paramagnetinių metalo jonų įterpimas į hibridines medžiagas yra įprasta praktika, leidžianti taikyti elektronų paramagnetinio rezonanso (EPR) metodus fazinių virsmų ir dinamikos tyrimams. Tačiau svetimų jonų įtraukimas į gardelę gali reikšmingai iškraipyti lokalią struktūrą, todėl medžiagos savybės gali būti interpretuojamos netiksliai. Mažiau invaziniai paramagnetiniai defektai gali būti suformuoti apšvitinant bandinį didelės energijos spinduliuote. Šiame darbe pateikiamas rentgeno spinduliais apšvitinto $[(CH_3)_2NH_2][Zn(HCOO)_3]$ hibridinio perovskito tolydžiosios bangos režimo (CW) EPR tyrimas; ši medžiaga pasižymi struktūriniu faziniu perėjimu ties ~160 K. CW EPR spektras atskleidžia rombinį $\boldsymbol{g}$ tenzorių be išskirtų hipersmulkiosios sąveikos signalų. Pasitelkę tankio funkcionalo teorijos (DFT) skaičiavimus, spektrą priskiriame radikalui, lokalizuotam formiato jungtyje. Išmatuotos g_{zz} komponentės temperatūrinė priklausomybė pasižymi plačia anomalija plačiame temperatūrų intervale netoli fazinio virsmo taško, kurią siejame su formiato jungties dinamikos pokyčiais.